PRESSURE STATISTICS IN HIGH-REYNOLDS NUMBER TURBULENT BOUNDARY LAYER

Yoshiyuki Tsuji[†‡], Jens H. M. Fransson[‡], P. Henrik Alfredsson[‡], and Arne V. Johansson[‡]

[†]Dept. Energy Engineering and Science,
Nagoya University, Nagoya 464-8603, Japan
c42406a@nucc.cc.nagoya-u.ac.jp

[‡]KTH Mechanics, Royal Institute of Technology,
100 44 Stockholm, Sweden

ABSTRACT

Static pressure fluctuations are an important ingredient in turbulence, e.g. in the pressure strain terms which redistribute turbulence among the different fluctuating velocity components. In the present study, both mean and fluctuating static pressure and wall pressure have been measured simultaneously in turbulent boundary layers. The pressure inside the boundary layer is measured with a specially designed probe. Results on mean and fluctuation distributions, spectra, Reynolds number dependence, and correlation functions are reported.

INTRODUCTION

There is an immense body of literature on the behaviour, distribution and scaling of velocity fluctuations in boundary layers, however so far very little is known about similar behaviour of pressure fluctuations. With regard to understanding the dynamics of turbulence such results are necessary, we only need to point out the importance of the pressure-strain terms which determine the redistribution of energy between the various velocity components. The main reason for the lack of such results is of course that no measurement technique so far has been able to actually measure pressure fluctuations inside the boundary layer. Recently Tsuji and Ishihara (2003) demonstrated the use of a specially designed probe which allows measurement of pressure fluctuations also inside a turbulent flow. In the present work we present new results obtained with similar probes which seem to be able to accurately measure not only the mean static pressure but also pressure fluctuations inside the turbulent boundary layer.

EXPERIMENTAL CONDITION

The experiments are performed in the MTL (Minimum Turbulence Level) wind tunnel at KTH. This is a high quality flow tunnel with a streamwise turbulence intensity of less than 0.025% at a free stream speed of 25 m/s and a total pressure variation less than 0.06% across the test section (see Lindgren, 2002 for further details about the MTL wind tunnel). The present experimental conditions are matched with those of Österlund (1999) which cover the Reynolds number range $2600 \leq R_\theta \leq 26700$.

The measurement station is set at 5.5 m from the leading edge. A specially designed traversing system protruding from the plate is used to position the probes. The probe position is changed in the range of $0 \leq y \leq 120$ mm.

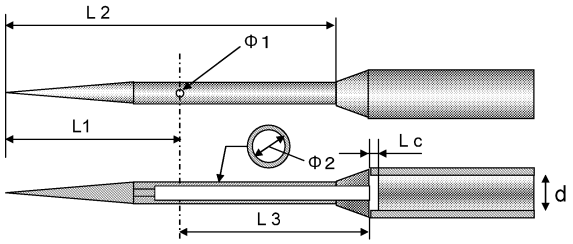

Figure 1: Schematic view of static pressure probe.

The measurement of pressure fluctuation in the flow field is accomplished with both a small piezo-resistive transducer and a standard quarter-inch condenser microphone. The transducer has a frequency response from D.C up to 150 kHz with a dynamic range of 3.5×10^3 Pa. The maximum errors contained in linearity and hysteresis are 0.25%. A microphone is available for measuring the frequency from 20 Hz up to 70×10^3 Hz. The lower frequency is restricted due to its mechanical system. The dynamic range is $2\times10^{-2} \sim 3.2\times10^3$ Pa, so a very small amplitude can be measured. The probe is a standard Pitot-static tube measuring ϕ_2 mm in inside diameter as indicated in Fig. 1, whereas the wall thickness of the tube is $h = 0.05$ mm.

Four static pressure holes (ϕ_1 mm in diameter) are spaced 90° apart and located at a distance of L_1 from the tip of the probe to minimize sensitivity to cross-flow error. The leeward end is terminated by the microphone or the transducer. The sensor diameters are $d_T = 1.6$ mm and $d_M = 7.0$ mm for the transducer and microphone, respectively. The transducer can detect low-frequency pressure fluctuations, but its sensitivity is fairly low, giving a measurable amplitude larger than 10 Pa. The microphone on the other hand can detect very small amplitudes, but frequencies below 10 Hz cannot be measured. In this experiment, five different tube diameters are used, listed in Table 1.

The fluctuating wall-pressure is measured by various configurations involving a pinhole in the boundary surface and by a piezoelectric transducer having a sensing element of the same diameter as the pinhole. According to Bull (1996), measurements are classified as (1) a condenser microphone mounted in a cavity behind the surface pinhole, (2) a piezo-electric transducer mounted behind the pinhole, (3) a piezo-electric

Table 1: Static tube and pinhole size.

	ϕ_1	ϕ_2	L_1	L_2	L_3
probe1	0.2	1.0	22.5	47.5	30.0
probe2	0.15	0.5	15.5	27.5	16.0
probe3	0.2	0.7	15.5	27.5	18.5
probe4	0.4	1.0	22.5	47.5	30.0
probe5	0.3	1.0	22.5	47.5	30.0

transducer mounted behind the pinhole, but with no cavity, (4) a piezo-electric transducer mounted behind the pinhole (with no cavity), but with the pinhole filled with silicone grease to restore a continuous boundary surface, (5) a piezo-electric transducer mounted flush with the boundary surface with no surface discontinuity. Analyzing the previously reported results, he concluded that the pinhole is responsible for local flow disturbances, which leads to errors in measured data. However, Farabee and Casarella (1991) concluded that pinhole sensors are effective for wall-pressure measurements. Thus, this problem appears to quite equivocal. Keith et al. (1992) pointed out the effect of sensor spatial resolution is of primary importance. In the present study wall pressure fluctuation is measured by techniques (1), (2), and (3). The pinhole diameter is $d = 0.3$ mm and its depth is $\ell = 1.0$ mm.

The streamwise velocity is measured by a single hot-wire operated in the constant-temperature anemometer mode. The hot-wire probe can be traversed to a minimum distance of 1.0 mm from the pinhole of the static pressure probe. The streamwise velocity and the static pressure are measured simultaneously. Also, the correlation between the static pressure and the wall pressure at different locations in the boundary layer is measured for several Reynolds numbers.

CALIBRATION OF STATIC PROBE

Yaw angle effect

The probes were inserted into the flow domain in such a way that the axis of the microphone (or the transducer) itself is aligned with the mean flow. We have preliminarily checked how the angle between the pressure probe and the flow direction affects the measured data. For this study the static probes were set in the potential core on the centreline of a round jet. The initial jet velocity is $U_J = 10$ m/s, and the probe is rotated within $-20 \leq \theta \leq +20$ degrees. The mean pressure is measured by a manometer (dynamic range is 50 Pa). The pressure coefficient defined as

$$C_P = (P_\theta - P_0) / \frac{1}{2}\rho U_J^2 , \qquad (1)$$

is plotted against the yaw angle in Fig. 2. Here, P_θ is the mean pressure at angle θ and P_0 is the mean pressure for $\theta = 0$. In the range of ± 5 degrees, the absolute value of C_P does not change with more than 0.001 for all probes used.

Mean pressure calibration

A mean pressure calibration of the probes is performed as follows. A Prandtl tube and the static probe are set parallel with each other in the potential core of a jet. Tygon plastic tubing, 2 m in length, is connected to the outlets of

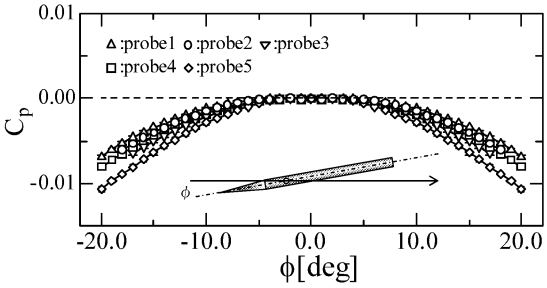

Figure 2: Yaw angle effect for static pressure probe.

both probes. The pressure difference between these, ΔP, is measured by a manometer with a dynamic range of 50 Pa. As plotted in Fig. 3, ΔP is very small for speeds less than 10 m/s but it is not negligible when U_J is larger than 20 m/s. For the probe with a diameter of $\phi_2 = 1.0$ mm the smallest orifice size makes ΔP negative, but the pressure difference becomes positive for the largest one. On the other hand, for the smallest probe 2, the pressure difference indicates the largest positive value. This indicates that ΔP might be a function of both the static tube size and the orifice size. Also, the 2 m long plastic tubing, which connects the static tube with the manometer, may have some influence.

The mean pressure profiles measured with all five probes across the boundary layer are shown in Fig. 4 for $R_\theta = 10460$. The measured pressure distributions collapse fairly well for all probes when the correction as mentioned above is made.

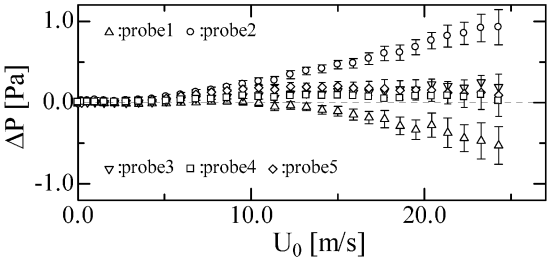

Figure 3: Pressure difference, ΔP, between the static pressure tube and the Prandtl tube.

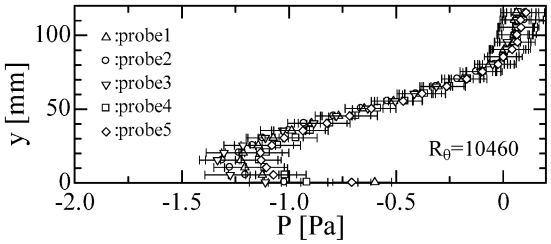

Figure 4: Static pressure distribution through the boundary layer measured with the five different sized probes.

Pressure fluctuation calibration

The probe is calibrated for measurements of static pressure fluctuations in the manner described below. The pressure probe is positioned parallel to the reference microphone and pressure fluctuations generated by a speaker are picked up by

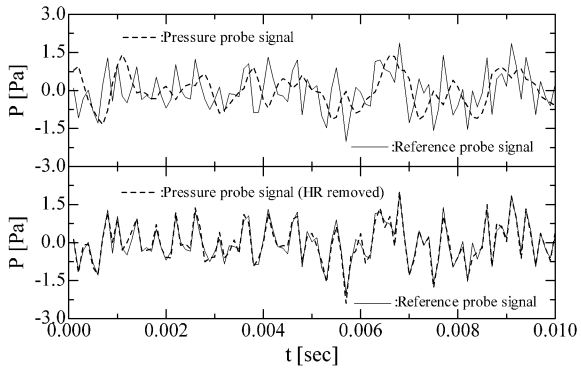

Figure 5: Illustration of the effect of removal of the HR. See text for details.

these two probes simultaneously. The output signal from the pressure probe, $p_s(t)$, differ however from the signal, $p_r(t)$, measured by the reference microphone. This is probably because of the attached static pressure tube and the Helmholtz resonance. Although the size of the pressure tube is small, this may also give a small effect on the measurement.

The frequency response of the system is limited by Helmholtz-resonator (abbreviated as HR) responses of the tube and sensor cavity (Kobashi, 1957, Toyoda, 1993). This HR frequency is calculated by

$$f_r = \frac{U_s}{2\pi}\sqrt{\frac{S}{L_3 V}}\,, \tag{2}$$

where V is the cavity volume, L_3 is the tube length, U_s is the speed of sound and S is the cross section (see also Fig. 1). For instance, with $V = \pi d^2 L_c/4$ m^3 and $S = \pi(\phi_2)^2/4$ m^2 the resonant frequency is 2.5 kHz and 11.1 kHz for the microphone (d = 7.0 mm, ϕ_2 = 1.0 mm, L_3 = 18.5 mm) and transducer (d = 1.6 mm, ϕ_2 = 1.0 mm, L_3 = 18.5 mm), respectively. Using the phase difference and the amplitude ratio between p_s and p_r in Fourier space, HR is numerically removed from p_s. A typical example is shown in Fig. 5. Although the original fluctuation p_s differs significantly from p_r, once the effect of HR is removed, those signals match each other excellently.

A standing wave inside the pressure probe may also cause a small disturbance to the pressure fluctuations. The frequency of the standing wave is given by $f_s = U_s/\lambda_s$ where $\lambda_s/4 = L_3$ and f_s is about 7.1 kHz for probe 1. The spatial resolution is estimated to be a few times the tube diameter. Then the corresponding frequency, $f_c = U_c/(n \times d)$, is taken into account in the measurements. Here, U_c is the local mean velocity, d is probe diameter, and n is to be from 2 to 5. f_c is the order of 10.0 kHz at U_c = 20.0 m/s.

Background noise

It is always difficult to achieve accurate measurements of pressure beneath the turbulent boundary layer due to signal contamination resulting from facility induced noise. For low Reynolds numbers, these acoustic disturbances, generally lower than 100 Hz, dominate the signal, however, noise contamination may be simply neglected when measurements are made at sufficiently high Reynolds numbers since the turbulent pressure fluctuations overwhelm the low-frequency disturbance.

The static pressure measured at y = 120 mm from the wall, $p_s(t)$, and the wall pressure fluctuation $p_w(t)$ are analyzed in order to evaluate the background noise. In this experiment, the boundary layer thickness is 65 mm at most. Therefore, the location y = 120 mm is twice the boundary layer thickness, and it is so far from the wall that there may be no correlation caused by turbulence between them. If p_s and p_w contain the same low frequency noise, they are divided as

$$p_s(t) = p'_s(t) + p_b(t)\,,\; p_w(t) = p'_w(t) + p_b(t)\,, \tag{3}$$

where $p_b(t)$ is a background noise due to acoustic noise and vibrations. p'_s and p'_w are expected true pressure fluctuation. The correlation function is calculated as

$$\langle p_s p_w \rangle = \left\langle p'_s p'_w \right\rangle + \left\langle p_b^2 \right\rangle\,, \tag{4}$$

because of the independence of p_b on the turbulent statistics. We can suppose $\langle p'_s p'_w \rangle \simeq 0$, because the static pressure is measured at $y \simeq 2\delta$. Then the root mean square of the background noise is $p_{b,rms} \equiv \sqrt{\left\langle p_b^2 \right\rangle} \simeq \sqrt{\langle p_s p_w \rangle}$. $p_{b,rms}$ increases as a function of Reynolds number like $p_{b,rms} \propto R_\theta^{1.98}$. When it is normalized by inner variables, $p_{b,rms}/\rho u_\tau^2$ decrease as Reynolds number increases and asymptotically approach the constant value of 0.7.

The frequency spectrum of p_s is shown in Fig. 6. It is noted that the low frequency noise appears smaller frequencies than 100 Hz. The sharp peak around 300 Hz may be caused by the acoustic noise emanating from the wind tunnel fan. It is concluded, therefore, that the low frequency noise contaminates the measured signal in the low frequency region, $f \leq 20$ Hz. In the high frequency region, say in the inertial range and in the dissipation range, acoustic noise effects are small. According to Kolmogorov's ideas turbulence at large Reynolds numbers has a spectrum which exhibits a simple form with the familiar $-5/3$ law for the velocity fluctuations in the inertial subrange. The corresponding exponent for the pressure spectrum becomes $-7/3$. The $-7/3$ power-law scaling was supported theoretically with various assumptions in the 1950's by Batchelor (1952), Inoue (1951), and Obukhoff & Yaglom (1953). Recently, Tsuji & Ishihara (2003) have examined the pressure spectrum in fully developed turbulence. In the spectra presented in Fig. 6 we cannot observe a substantial inertial range. The slope of the line in the figure is -1.5.

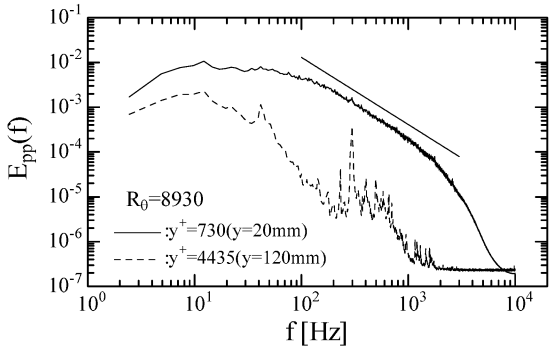

Figure 6: Static pressure spectrum measured in the boundary layer at y = 20 mm and in the free stream region, y = 120 mm. Slope of solid line is -1.5.

The reason for this may be that the Reynolds number is too low in order to have a substantial inertial range. Future work aims to clarify this issue.

We also compute the correlation function with time lag τ, $\langle p_s(t+\tau)p_w(t)\rangle$. If the Taylor hypothesis is adopted, it indicates the correlation between wall pressure and the static pressure at a distance $U_0 \times \tau$ upstream from the wall pinhole. The correlation coefficient $C_\tau \equiv \langle p_s(t+\tau)p_w(t)\rangle / (p_{s,rms}p_{w,rms})$ decreases and it is almost zero for large separation distance, 2.0 m $\leq \tau U_0$. Thus, the low frequency noise is associated with motions of a few meters in space.

RESULTS AND DISCUSSIONS

Mean pressure profile

The mean pressure distribution measured by probe1 is plotted in Fig. 7. The distance from the wall, y, is normalized by Rotta-Clauser boundary layer thickness Δ, and the pressure in the boundary layer $P(y)$ is subtracted from the pressure in the free stream region. That is, $P(y)$ is always smaller than P_0. Note here that the mean pressure is affected by the wall up till $y \simeq 0.3\Delta$ and that the peak of $\Delta P_M = P_0 - P$ is located around $y \simeq 0.05\Delta$. The boundary layer thickness, δ, is roughly evaluated to be 0.2Δ, and it is then concluded that the mean pressure effect remains far from the wall. It is similar to the vertical-component velocity characteristic.

The boundary layer momentum equation normal to the plate shows that the mean static pressure $P(y)$ varies with the distance from the wall (y) as

$$P(y)/\rho = P_0/\rho - \left\langle v^2 \right\rangle , \qquad (5)$$

where P_0 is the mean pressure in the free-stream and v is the velocity fluctuation component normal to the plate. The rms-distributions of the normal velocity calculated from the above relation, normalized by inner variables are plotted in Fig. 8. The normalized fluctuation level, $\sqrt{\langle v^2\rangle}/u_\tau$, is slightly larger than what is expected from direct v-measurements but the profiles are quite similar (cf. Österlund, 1999). This discrepancy can, however, be explained by the uncertainty of $\Delta P_M \simeq O(10^{-1})$ Pa. Also, the calibration curve is only to evaluate the relative errors. There is still an uncertainty of how accurately the Prandtl tube pick up the mean static pressure. Possible effects of plastic tubing connected to the outlet is also not considered here. If the peak position of $\sqrt{\langle v^2\rangle}/u_\tau$ is expressed as y_p^+, its Reynolds number dependence is plotted in the inset. The peak position is scaled by the relation, $y_p^+ = 0.00135 \times R_\theta^{1.42}$. The dashed line is given by Fernholz & Finley (1996), which represents $y_p^+ = 0.071 \times R_\theta$.

Root mean square of static and wall pressure fluctuations

In Fig. 9 the root mean square (rms) of the static pressure is plotted against the distance from the wall. The contribution from the background noise evaluated by Eq. (4) is removed. The Reynolds number varies in the range $5880 \leq R_\theta \leq 15210$. When the distributions are normalized with outer scales there is an almost perfect collapse between the different Reynolds numbers. This shows a strong influence of the outer scales on the pressure fluctuations. Direct numerical simulation (Skote, 2001) shows that p_{rms} has a maximum around $y^+ \simeq 30$. Since the peak is located very close to the wall, it is not possible to resolve in the present experiments due to direct probe interaction with the wall. Our hypothesis is however, that also close to the wall we would find an outer scaling of the pressure fluctuations.

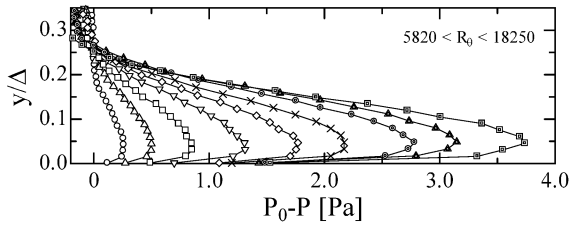

Figure 7: Mean static pressure profiles in the boundary layer. P_0 is the mean pressure in the free stream. The distance from the wall y is normalized by Rotta-Clauser thickness Δ.

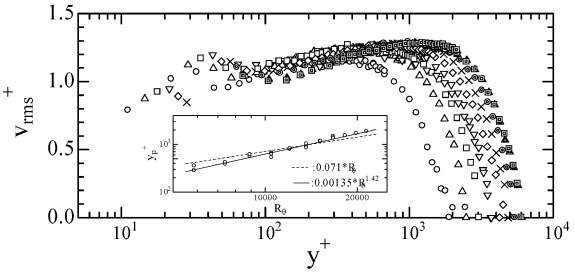

Figure 8: Root mean square of vertical velocity fluctuation computed by Eq. (5). Inset shows the peak position of v_{rms}^+ as a function of Reynolds number.

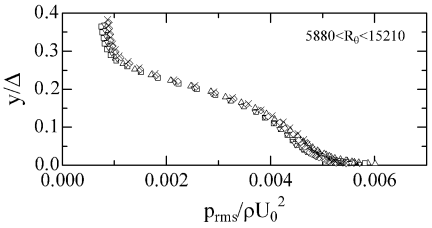

Figure 9: Root mean square of static pressure fluctuations, normalized by the free stream variables, versus the distance from the wall normalized by the Rotta-Clauser thickness, Δ, for $5880 \leq R_\theta \leq 15310$.

There are many reports about wall pressure measurement (Schewe, 1983, Gravante et al. 1998, Löfdahl & Gad-el-Hak, 1999, and references therein). According to the previous reports, a pressure recorded by the pinhole is higher than "true" values at the wall. The pressure error, Δp_w = (measured value)–(true pressure), may depend on pinhole diameter d, hole depth ℓ, the diameter of the connection to the manometer d_c, the wall shear stress τ_w, kinematic viscosity ν, and the characteristic length scale of the facility, D. Thus, the static pressure error for a finite hole size can be written as

$$\Pi = \frac{\Delta p_w}{\tau_w} = f\left(\frac{du_\tau}{\nu}, \frac{d}{D}, \frac{\ell}{d}, \frac{d_c}{d}\right) , \qquad (6)$$

where u_τ is the friction velocity and Π is the non-dimensional

pressure error (Shaw, 1960). As Shaw noted, the error is always positive but it becomes zero for very small d. He also found that the non-dimensional pressure error, Π, increases with increasing d^+ but reaches an asymptotic limit $\Pi \simeq 2.7$ at $d^+ = 800$. The error increases with the ℓ/d ratio but there is no further change with ℓ/d when ℓ/d approaches $1.5 \sim 2$. In the present experiment, the normalized pinhole diameter changes from $4.6 \leq d^+ \leq 20.7$ to $\ell/d = 3.33$, thus the error may be very small.

The rms of the wall pressure, where the background noise evaluated by Eq. (4) is removed, is plotted in Fig. 10 normalized by inner variables. The rms-levels are of the same order as the static pressure variations in the boundary layer, and the Reynolds number dependence is well approximated by a power law with exponent 0.28. A similar trend is also observed in DNS-data obtained by Skote (2001). When $(p^+_{rms})^2$ is plotted against δ^+, the present results scatter around the relation reported by Farabee and Casarella (1991); ${p^+_{rms}}^2 = 6.5 + 1.86\ln(\delta^+/333)$, and shows a stronger Reynolds number dependence indicating a scaling close to outer scaling.

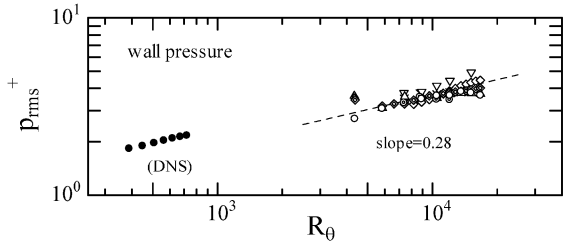

Figure 10: Root mean square of the wall pressure, normalized by inner variables, as a function of Reynolds number. DNS values are obtained by Skote (2001).

The wall pressure spectra normalized by inner variables are shown in Fig. 11. The high frequency region of the spectra is seen to approximately scale on inner variables. Bradshaw (1967) predicts a region where spectra collapse on both inner and outer variables. This region exhibits an ω^{-1} behavior, which can be associated with pressure sources in the logarithmic part of boundary layer. The current results show a significant portion of the spectra exhibits a power-law behavior, but with a slope of -0.7. Before putting to much emphasis of these results a more thorough investigation on spatial resolutions issues has to me made. Such results will be discussed in future publications.

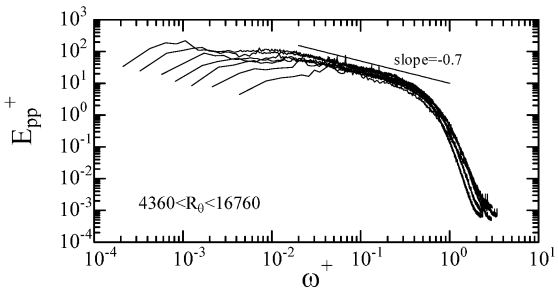

Figure 11: Wall pressure spectra normalized by inner variables.

Correlation between static and wall pressure fluctuations

The correlations measured between the wall pressure and the static pressure inside the boundary layer are plotted in Fig. 12 for different Reynolds numbers. The background noise evaluated by Eq. 4 is removed from the measured data. One may conclude first that a positive correlation is observed across the boundary layer. Secondly there is no significant Reynolds number dependence for $Re_\theta > 7000$ when the distance from the wall is scaled with Δ.

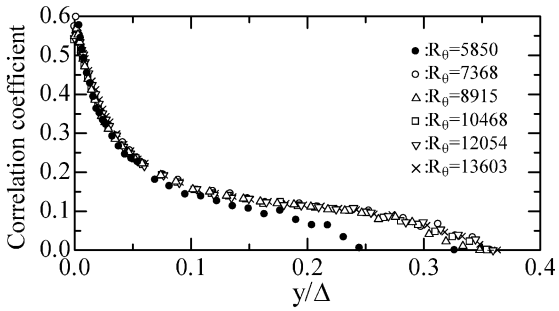

Figure 12: Correlation coefficient between wall pressure and static pressure in the boundary layer.

Velocity and pressure correlation

Subject to the quasi-normal assumption, fourth-order velocity structure functions are represented by products of factored second-order quantities. Therefore, the root mean square of pressure, p_{rms}, is scaled by $\rho {u_{rms}}^2$, i.e. $p_{rms}/\left(\rho {u_{rms}}^2\right) = C_1$. Hinze (1975) suggested that C_1 is 0.7 whereas Batchelor (1951) gave a value of $C_1 = 0.58$. In the course of this study, C_1 is found to be dependent on the distance from the wall. But it is close to $O(1)$ in the overlap region (see Fig. 13). These results are in qualitative agreement with DNS results by Skote (2001).

Correlations between the pressure and the streamwise velocity fluctuations through the boundary layer are plotted in Fig. 14. We can find three significant features. Firstly, the correlation reaches a local minimum value close to the wall, around $y/\Delta \simeq 0.05$. Secondly, the maximum correlation is located around the boundary layer thickness, $y \simeq 0.2\Delta$. This value decreases as the Reynolds number increases. Thirdly, the correlation becomes negative in the free-stream region. The latter result may be explained by the Bernoulli equation. These three features are also observed in the DNS by Skote (2001). We believe that the second characteristic may be used to distinguish the turbulent and non-turbulent boundary in-

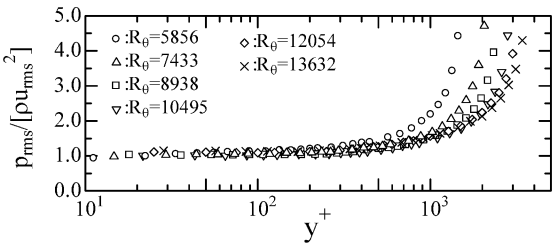

Figure 13: Root mean square of pressure normalized by ρu^2_{rms}.

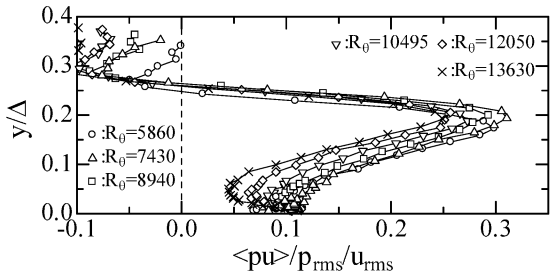

Figure 14: Correlation between stream-wise velocity and static pressure in the boundary layer.

terface. Work along this line will be reported in the near future.

CONCLUSIONS

In this experiment, both the mean and fluctuating static pressure and wall pressure are measured in high-Reynolds number turbulent boundary layer flows. No previous measurements inside a turbulent boundary layer are known to the authors. The results may be summarized as follows.

1. The root mean square of the vertical velocity component $\sqrt{\langle v^2 \rangle}$ is evaluated by means of mean pressure distribution with Eq. (5). The profile agrees fairly well with results obtained by direct v-component velocity measurement.

2. The root mean square of wall pressure, normalized by the square of the friction velocity, indicates an increasing function of R_θ; $p^+_{rms} \propto R_\theta^{0.28}$. This trend is similar with result from DNS at lower Re and indicates an approximate scaling with outer variables, i.e. a dominate influence of outer scales on the pressure fluctuations even in the near wall region.

3. The distribution of static pressure rms, p_{rms}, across the boundary layer is almost constant, independent of Reynolds number if scaled with outer variables. This is in accordance with the results for the wall pressure fluctuations.

4. The distributions of the correlation coefficient between wall and static pressure across the boundary layer for different Reynolds numbers ($R_\theta > 7000$) essentially collapse if the distance from the wall is normalized by Δ.

5. The ratio $p_{rms}/\rho u^2_{rms}$ is about 1 in the inner and overlap regions. The correlation between the pressure and streamwise velocity exhibits local minimum and maximum values at $y/\Delta \simeq 0.05$ and $y/\Delta \simeq 0.2$, respectively. Just outside the boundary layer, $y/\Delta > 0.25$, the correlation becomes negative, probably because potential flow disturbances generate a negative correlation. These trends are also observed in DNS.

The stay at KTH by YT was supported by the Royal Academy of Sciences through an exchange program in cooperation with JSPS. JHMF was supported through a grant from the Swedish Research Council (VR). We are grateful to Dr. M. Skote for his comments during the experiments and for providing DNS-results for comparison.

REFERENCES

Batchelor, G. K. 1951 "Pressure Fluctuations in Isotropic Turbulence", *Proc. Camb. Phil. Soc.*, vol. 47, pp. 359–374.

Bradshaw, P. 1967 "Inactive Motion and Pressure Fluctuation in Turbulent Boundary Layers",*J. Fluid Mech.*, vol. 30, pp. 241–258.

Bull, M. K. 1996 "Wall-pressure Fluctuations beneath Turbulent Boundary Layers: Some Reflections on Forty Years of Research", *J. Sound and Vibration*, vol. 190, pp. 299–315.

Farabee, T. M. and Casarella, M. J. 1991 "Spectral Features of Wall Pressure Fluctuations beneath Turbulent Boundary Layers", *Phys. Fluids*, vol. 3, pp. 2410–2420.

Fernholz, H. F. and Finley, P. J. 1996 "The Incompressible Zero-pressure-gradient Turbulent Boundary Layer: An Assessment of the Data", *Prog. Aerospace Sci.*, vol. 32, pp. 245–311.

Gravante, S. P., Naguib, A. M., Wark, C. E. and Nagib, H. M. 1998 "Characterization of the Pressure Fluctuations under a Fully Developed Turbulent Boundary Layer", *AIAA J.*, vol. 36, pp. 1808–1816.

Hinze, J. O. 1975 *Turbulence*, McGraw-Hill.

Inoue, E. 1951 "The Application of the Turbulence Theory to the Large-Scale Atmospheric Phenomena", *Geophys. Mag.*, vol. 23, pp. 1–14.

Keith, W. L., Hurdis, D. A. and Abraham, B. M. 1992 "A Comparison of Turbulent Boundary Layer Wall-Pressure Spectra", *J. Fluids Engng.*, vol. 114, pp. 338–347.

Kobashi, Y. 1957 "Measurements of Pressure Fluctuation in the Wake of Cylinder", *J. Physical Soc. Japan*, vol. 12, pp. 533–543.

Löfdahl, L. and Gad-el-Hak, M., 1999 "Mems-based Pressure and Shear Stress Sensors for Turbulent Flow", *Meas. Sci. Technol.*, vol. 10, pp. 665–686.

Lindgren, B., 2002 "Flow Facility Design and Experimental Studies of Wall-bounded Turbulent Shear-flow", Doctoral thesis, Royal Institute of Technology.

Österlund, J.M., 1999 "Experimental Studies of Zero Pressure-gradient Turbulent Boundary Layer Flow", Doctoral thesis, Royal Institute of Technology.

Österlund, J. M., Johansson, A. V., Nagib, H. M. and Hites, M. H., 2000 "A note on the Overlap Region in Turbulent Boundary Layers", Phys. Fluids, vol. 12, pp.1–4.

Obukhoff, A. M. and Yaglom, A.M., 1951 "The Microstructure of Turbulent Flow", *NACA TM* 1350.

Schewe, G. 1983 "On the Structure and Resolution of Wall-pressure Fluctuations associated with Turbulent Boundary-layer Flow" *J. Fluid Mech.*, vol. 134, pp. 311–328.

Shaw, R. , 1960 "The Influence of Hole Dimensions on Static Pressure Measurements", *J. Fluid Mech.*, vol. 7, pp. 550–564.

Skote, M., 2001 "Studies of Turbulent Boundary Layer Flow through Direct Numerical Simulation", Doctoral thesis, Royal Institute of Technology.

Tsuji, Y. and Ishihara, T., 2003 "Similarity Scaling of Pressure Fluctuation in Turbulence", *Phys. Rev. E*, Vol. 68, 026309.

Toyoda, K., Okamoto, T. and Shirahama, Y. 1993 "Eduction of Vortical Structures by Pressure Measurements in Noncircular Jet", *Fluid Mechanics and its Applications*, vol. 21, pp. 125–136.